FULL-LENGTH PAPER

THE PROTEIN SOCIETY WILEY

Activity and substrate specificity of lytic polysaccharide monooxygenases: An ATR FTIR-based sensitive assay tested on a novel species from *Pseudomonas putida*

Ilenia Serra[1] | Daniele Piccinini[1] | Alessandro Paradisi[1,2] | Luisa Ciano[3] |
Marzia Bellei[1] | Carlo Augusto Bortolotti[1] | Gianantonio Battistuzzi[3] |
Marco Sola[1] | Paul H. Walton[2] | Giulia Di Rocco[1]

[1]Department of Life Sciences, University of Modena and Reggio Emilia, Modena, Italy

[2]Department of Chemistry, University of York, York, UK

[3]Department of Chemistry and Geology, University of Modena and Reggio Emilia, Modena, Italy

Correspondence
Giulia Di Rocco, Department of Life Sciences, University of Modena and Reggio Emilia, via Campi 103, Modena 41125, Italy.
Email: giulia.dirocco@unimore.it

Present address
Ilenia Serra, BIMEF Laboratory, Department of Chemistry, University of Antwerp, Antwerp, Belgium

Luisa Ciano, School of Chemistry, University of Nottingham, Nottingham, UK

Funding information
Biotechnology and Biological Sciences Research Council, Grant/Award Numbers: BB/L001926/1, BB/L021633/1; University of Modena and Reggio Emilia, Grant/Award Number: FARDSV 2019 Di Rocco

Abstract

Pseudomonas putida W619 is a soil Gram-negative bacterium commonly used in environmental studies thanks to its ability in degrading many aromatic compounds. Its genome contains several putative carbohydrate-active enzymes such as glycoside hydrolases and lytic polysaccharide monooxygenases (PMOs). In this study, we have heterologously produced in *Escherichia coli* and characterized a new enzyme belonging to the AA10 family, named *Pp*AA10 (Uniprot: B1J2U9), which contains a chitin-binding type-4 module and showed activity toward β-chitin. The active form of the enzyme was produced in *E. coli* exploiting the addition of a cleavable N-terminal His tag which ensured the presence of the copper-coordinating His as the first residue. Electron paramagnetic resonance spectroscopy showed signal signatures similar to those observed for the copper-binding site of chitin-cleaving PMOs. The protein was used to develop a versatile, highly sensitive, cost-effective and easy-to-apply method to detect PMO's activity exploiting attenuated total reflection-Fourier transform infrared spectroscopy and able to easily discriminate between different substrates.

KEYWORDS
activity, ATR FTIR spectroscopy, chitin, EPR, lytic polysaccharide monooxygenase

1 | INTRODUCTION

Polysaccharide monooxygenases (PMOs) are copper-dependent redox enzymes currently divided into eight families of auxiliary activity (AA) enzymes (AA9–AA11 and AA13–AA17) in the Carbohydrate-Active EnZYmes database (http://www.cazy.org/).[1,2] Since their discovery in 2010,[3] an increasing number of PMOs from diverse organisms has been identified, encompassing a broad substrate specificity which includes chitin, cellulose,[4] hemicelluloses,[5,6] starch,[7] and even homogalacturonan.[8] PMOs thus carry out oxidation of recalcitrant biopolymers in an O_2 and electron-dependent process, helping the breakdown of lignocellulosic biomasses by canonical

chitinases and cellulases[9–11] and reducing the required amount of enzymatic cocktails for industrial degradation. For this reason, these enzymes have attracted extensive research focused on their fundamental chemical and biochemical properties, in the view of industrial exploitation.[12,13] The active site of these enzymes is solvent-exposed and contains a mononuclear copper ion coordinated by an N-terminal histidine along with the side chain of a second histidine, generating a T-shaped configuration known as the histidine brace (Figure 1).[14,15]

Despite substantial effort in the investigation of the physico-chemical properties of PMOs active-site and numerous studies focused on their activity, some aspects of their reaction mechanism remain unclear.[4,9] Furthermore, the insoluble nature of these biopolymers hinders the use of routine biochemical analysis methods, which typically require homogenous conditions. Recent studies showed that PMOs utilize either O_2 or H_2O_2 as co-substrates[16–18] and the quantification of H_2O_2 has been often used to indirectly determine PMO activity.[19] Alternatively, activity measurements rely on the identification of soluble oligosaccharides which are released following the PMO activity on the complex biomasses, such as in the case of the kinetic analysis made on a ^{14}C-labelled substrate,[17] while other methods are based on the spectroscopic quantitation of a colored pyrocatechol–Ni^{2+} complex[17,20,21] or a dimer product named coerulignone.[22,23] Traditionally, PMOs activity is analyzed by modern liquid chromatography and mass spectrometry methods, however continuous developments in research on PMOs and other carbohydrate-active redox enzymes will require an expanded repertoire of screening methods able to detect a wider range of products.[24] While these homogeneous assays may be used as a probe for PMO activity, they do not give information on the reaction kinetics with native, heterogeneous PMO substrates. Nevertheless, the use of the natural substrate is fundamental to prevent protein deactivation, which has been shown to affect the results of the assay.[25–27] Despite the availability of numerous studies focused on enzyme production processes, sensitive, cost-effective and easy-to-apply method to detect PMO activity and to discriminate between substrates has yet to be developed. In this context, we describe here a simple, versatile, and sensitive assay for the assessment of PMO activity and substrate specificity using attenuated total reflection-Fourier transform infrared (ATR-FTIR) spectroscopy.

A new bacterial enzyme active on chitin, that is, the monomeric putative PMO from *P. putida* W619 (*Pp*AA10 hereafter), was produced in *Escherichia coli*, characterized with spectroscopic and mass spectrometry techniques and used as model system in order to develop and test the above-mentioned activity assay.

2 | RESULTS AND DISCUSSION

2.1 | Production and purification of *Pp*AA10

The successful cloning of the expression vector into *E. coli* DH5α cells and the subsequent transformation of *E. coli* BL21(DE3) cells were confirmed by colony PCR. Figure S1a shows the results of DNA gel electrophoresis where a band between 750 and 1,000 base pairs (bps) can be observed, corresponding to the expected length of 927 bps of the *PpAA10*-pLATE52 construct. The recombinant *Pp*AA10 protein was then produced on a large scale and purified by affinity chromatography. SDS-PAGE of the eluted protein (Figure S1b, lane 3) shows a high degree of purity, since only one band at 25 kDa is visible, which is consistent with the expected molecular mass of *Pp*AA10 (see below). The same figure (lanes 1 and 2) depicts the digestion of *Pp*AA10 by the WELQut® enzyme, necessary to obtain the active form of the protein. The assay reveals the dependence of the cleavage efficiency on the chosen conditions and confirms the expected molecular weight of 21.9 kDa of the mature
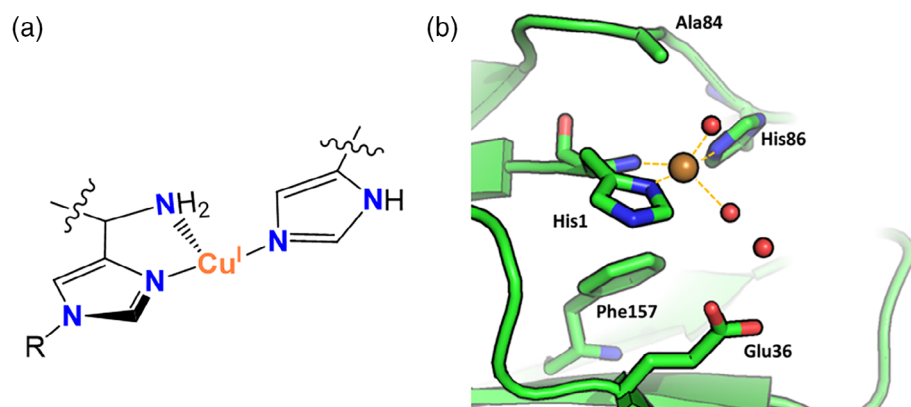
(a)

(b)

FIGURE 1 (a) Scheme of the copper histidine brace highlighting the T-shaped coordination geometry in the Cu(I) state (R = Me or H, depending on the PMO family considered). (b) X-ray structure of the Cu(II) resting state of the *Enterococcus faecalis* AA10 PMO (PDB 4ALC) showing the Cu(II) resting state coordination geometry, with the two exogenous H_2O ligands (red spheres) and several distal residues conserved in the AA10 family

*Pp*AA10 after the cleavage. The presence of a single band in the sample prepared with a ratio WELQut® enzyme/protein of 1:50 (Figure S2b, lane 2) demonstrates that the final sample is pure and homogeneous. The bands from the above-mentioned gel were extracted, digested with trypsin and analyzed via ESI-MS/MS spectrometry. Theoretical molecular masses of the undigested and digested *Pp*AA10 estimated with Expasy ProtParam tool, are 25,014.84 and 21,908.40 Da, respectively. Peptide mass fingerprint was carried out with MASCOT search engine, which yielded 44%–86% coverage for different sequences. In particular, tryptic peptides from the mature form of *Pp*AA10 after His-tag removal, showed a sequence coverage of 69% thus confirming the identity of the protein (Figure S2). The MS/MS of the 398.7202 *m/z* spectrum ([M + 2H$^+$]) corresponding to a molecular mass of 759.4239 Da for the N-terminal peptide HGSIASPK confirmed His as the first amino acid.

2.2 | Electron paramagnetic resonance spectroscopy

CW X-band electron paramagnetic resonance (EPR) spectroscopy in frozen solution was performed to investigate the electronic structure of the Cu(II) active site of *Pp*AA10. Initially, a spectrum collected at pH 7.0 revealed the presence of a mixture of two contributions and intense superhyperfine features in the g_x/g_y region of the spectrum ($B \sim 320$ mT). However, when the pH was lowered to 5.0, a single rhombic signal ($g_x < g_y < g_z$) was obtained without resolved superhyperfine coupling

(Figure 2a). For this species, herein referred as Species 1, accurate determination of the EPR parameters was only possible for the g_z and Cu $|A_z|$ values ($g_z = 2.257$; $|A_z| = 123 \times 10^{-4}$ cm^{-1}) but not for those of the g_x/g_y region. However, a good fitting of the experimental spectrum was obtained with $g_x = 2.02$, $g_y = 2.11$, $|A_x| = 73 \times 10^{-4}$ cm^{-1} and $|A_y| = 28 \times 10^{-4}$ cm^{-1} and with the inclusion of the three nitrogen ligands coupling, with an isotropic coupling (A_{iso}^N) of about 12×10^{-4} cm^{-1}. These EPR parameters are consistent with a distorted square pyramidal geometry in which the SOMO has a prevalent $d(x^2 - y^2)$ character, with a certain degree of $d(z^2)$ mixing., as previously reported for other AA10 PMOs.[30–32]

To evaluate a possible role of pH in the formation of the second species, herein denoted as Species 2, a pH titration in the range 5.0–9.5 was performed. Upon increasing the pH, Species 1, with predominant rhombic character, progressively converted into Species 2, characterized by axial features, suggesting a change in the overall Cu coordination geometry (Figure 2b). The relative amounts of the two contributions at each pH value are reported in Table S1, revealing a pK_a of 6.6–6.8 (see Figure S3 for a graphical representation). Species 2 shows axial EPR parameters consistent with a square planar geometry with little $d(z^2)$ mixing. An $|A_z|$ value of 187×10^{-4} cm^{-1} and a g_z value of 2.233 were accurately simulated for the spectrum acquired at pH 8.5 (Figure 2C and Figure S4). The spectrum reveals also a strong "overshoot" feature in the g_x/g_y region, which is the consequence of the combination of a very large $|A_z|$ value and a low g_z value. Again, a good fitting of the experimental
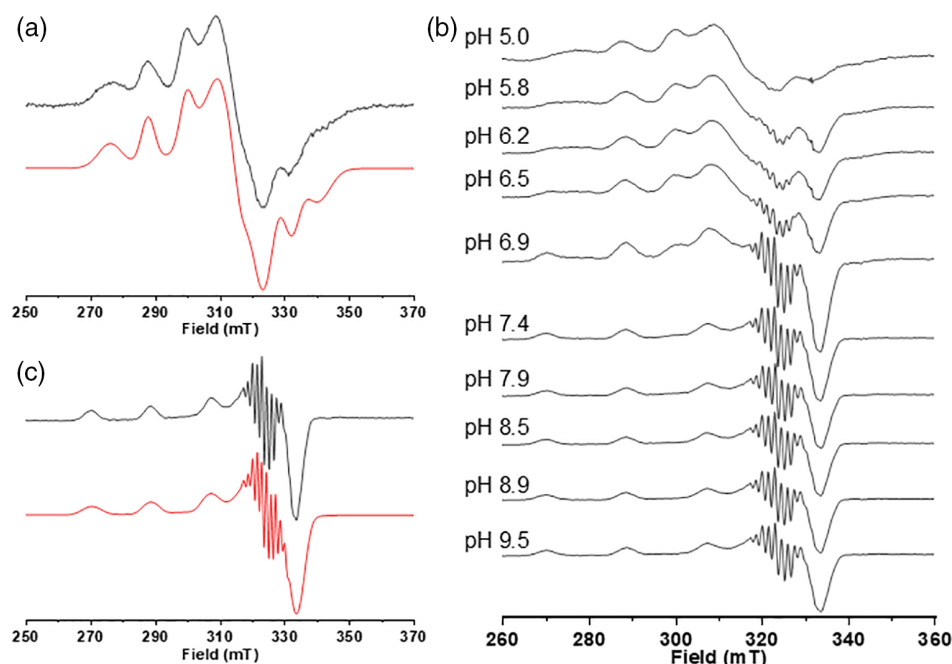

FIGURE 2 (a) X-Band (9.28 GHz, 170 K) CW EPR spectrum (black) and simulation (red) of *Pp*AA10 at pH 5.0. (b) X-band CW EPR spectra of *Pp*AA10 at different pH values. (c) X-band CW EPR spectrum (black) and simulation (red) of *Pp*AA10 at pH 8.5. Enzyme concentration was 0.21 mM in a 10 mM sodium acetate, 10 mM MES, 10 mM HEPES, 10 mM TRIS, 10 mM CHES, and 200 mM NaCl multi-buffer solution

spectrum was obtained with $g_x = 2.04$, $g_y = 2.05$, $|A_x| = 20 \times 10^{-4}$ cm^{-1}, $|A_y| = 17 \times 10^{-4}$ cm^{-1} and including the coupling of two nitrogen ligands with an isotropic coupling of about 12×10^{-4} cm^{-1} and with a Cl$^-$ ion with an isotropic coupling of about 15×10^{-4} cm^{-1} (Figure 2c and Figure S4). The intense superhyperfine coupling pattern in the g_x/g_y region allowed a more reliable estimation of the ligand super-hyperfine coupling values with respect to the low pH species; the obtained values are consistent with the values reported in literature for sp^2 nitrogen atoms[33] and Cl$^-$ ligands.[34] On the other hand, an alternative fit of the superhyperfine features of equivalent quality could be obtained including a third N ligand atom in place of the Cl$^-$, but only if an A_{iso}^N of $\sim 15 \times 10^{-4}$ cm^{-1} was allowed in the simulation. However, this value is significantly higher with respect to the typical nitrogen couplings (A_{iso}^N of 11–12 $\times 10^{-4}$ cm^{-1}) observed in LPMO enzymes and therefore difficult to justify with the available experimental data.[32,35] The EPR parameters of both PpAA10 forms fall in the range reported in the literature for other AA10s containing a type II copper center (Table S2). Interestingly, in the Peisach−Blumberg plot[36] (Figure S5) chitin-active AA10s are clustered around PpAA10 and share a conserved phenylalanine near the copper center, which is expected to be present also in PpAA10 from sequence analysis (Figure S6). Moreover, the distorted geometry of Species 1 is consistent with the coordination of one or two water molecules residing out of the plane defined by the histidine brace (Figure 1b), as shown for other AA10s by spectroscopic and structural studies.[30-32,35] The formation of Species 2 may arise from two processes: the replacement of a copper-coordinating water molecule by a Cl$^-$ ion from the buffer, or the deprotonation of a Cu(II)-bound water molecule to give an hydroxide ion ligand or the coordination to the Cu(II) of a distal residue, triggered by a protein conformational change. The only distal residue that could act as a ligand for Cu(II) is the Glu36; however, in the available AA10 PMO X-ray structures, this residue is generally positioned too far away from the metal to form a bond (~ 5 Å) without a significant structural change of the enzyme structure.

The presence of multiple species in the resting state EPR spectrum of another AA10 LPMO (*Streptomyces lividans* AA10E, or *Sl*AA10E) at pH 7.0 was also reported by Chaplin et al.[37] They suggested that the second species could arise from a chloride ion from the buffer solution binding to the Cu(II) on the basis of its $g_z = 2.23$, which they found similar to the one determined for another AA9 PMO with a Cl$^-$ acting as the exogenous ligand on Cu(II).[34] The g_z and $|A_z|$ values determined for Species 2 in PpAA10 are similar to those reported for the minor

species of *Sl*AA10E, as reported in Table S2, therefore supporting the chloride ligation hypothesis. However, a detailed investigation of the pH dependence of the Cu(II) coordination sphere is beyond the scope of this work and it will be the subject of more detailed future studies.

2.3 | MALDI-TOF assays

PMOs break down glycosidic bonds of polysaccharides with an oxidative mechanism, producing soluble oligosaccharides with different degrees of polymerization and specific chain-end modifications.[38] From its sequence similarity with other members of the AA10 family, PpAA10 was expected to be active on chitin. Therefore, α- and β-chitin were employed as substrates for this assay. The protein showed clear activity on β-chitin with the formation of C1-aldonic acids identified in the matrix assisted laser desorption Ionisation coupled to a time of flight analyser (MALDI-TOF) mass spectrum as the mono- or di-sodium adducts, although smaller peaks for the mono-sodium unopened lactone were also identified (Figure 3). No enzymatic activity on α-chitin was detected.

2.4 | ATR-FTIR spectroscopy assay

The MALDI-TOF analysis of the products from the enzymatic activity demonstrated that PpAA10 is a PMO able to oxidize β-chitin and to produce soluble oxidized oligosaccharides. Therefore, this enzyme was used as a model system to develop a new activity assay based on ATR-FTIR spectroscopy, to detect the release of these oligosaccharides in the solution. Figure S7 summarizes the key steps involved in the sample preparation and reaction products analysis (see Section 4 for the details of the procedure). Briefly, β-chitin was incubated with the enzyme and ascorbic acid (AA; used as reducing agent) for 24 h, then the excess of insoluble substrate was removed from the reaction mixture by centrifugation. A sample of the supernatant solution was then deposited on the ATR crystal and dried with air, before recording the IR spectrum.

As a preliminary step, the spectrum of β-chitin powder was collected to identify the spectral fingerprints of this polysaccharide and therefore be able to compare it with the spectra of the digested samples. Figure 4a shows the spectra of β-chitin (black line), the digestion supernatant (blue line) of the reaction mixture prepared with β-chitin, PpAA10 and AA, together with two supernatants from the control samples: one obtained without addition of
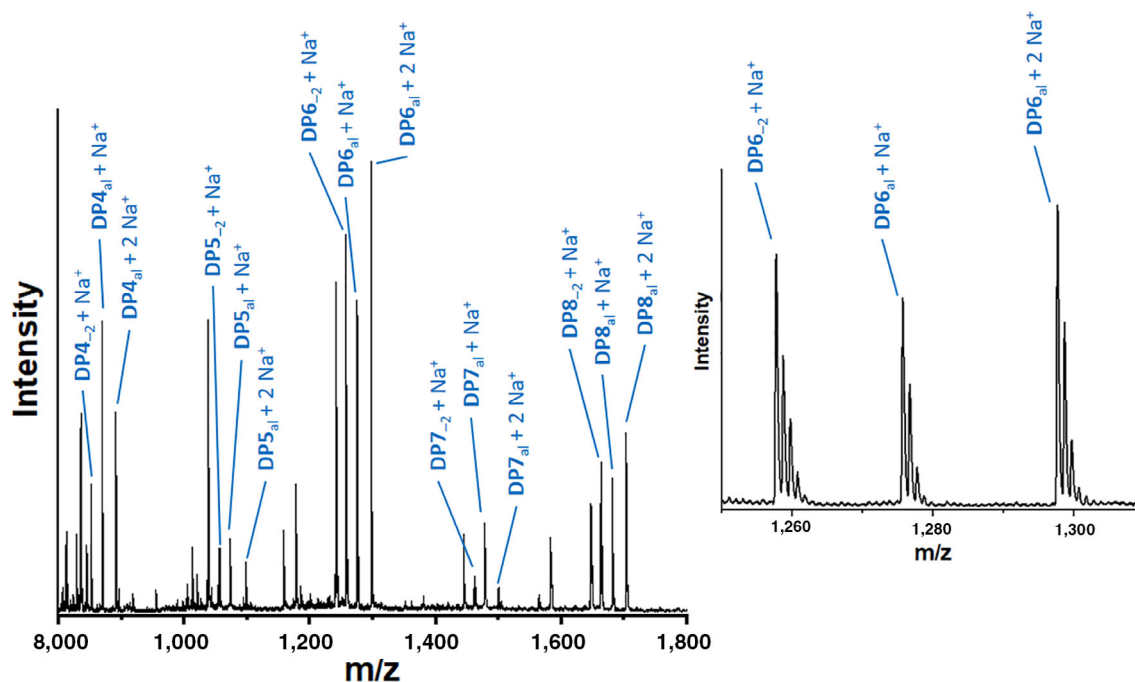
FIGURE 3 MALDI-TOF spectrum of reaction products of *Pp*AA10 activity on β-chitin from squid pen. DPn stands of degree of polymerization; DPn$_{al}$ aldonic acid; DPn$_{-2}$ aldonolactone form (measured molecular weight in Da). Reaction products are detected as sodium adducts. DP4$_{-2}$ + Na$^+$ (852.5), DP4$_{al}$ + Na$^+$ (869.5), DP4$_{al}$ + 2Na$^+$ (891.5), DP5$_{-2}$ + Na$^+$ (1,054.5), DP5$_{al}$ + Na$^+$ (1,072.9), DP5$_{al}$ + 2Na$^+$ (1,098.6), DP6$_{-2}$ + Na$^+$ (1,257.7), DP6$_{al}$ + Na$^+$ (1,275.7), DP6$_{al}$ + 2Na$^+$ (1,297.6), DP7$_{-2}$ + Na$^+$ (1,460.8), DP7$_{al}$ + Na$^+$ (1,478.7), DP7$_{al}$ + 2Na$^+$ (1,500.8), DP8$_{-2}$ + Na$^+$ (1,663.9), DP8$_{al}$ + Na$^+$ (1,681.9), and DP8$_{al}$ + 2Na$^+$ (1704.9). The inset shows an expansion of the DP6 region of the mass spectrum, highlighting the three main reaction products

*Pp*AA10 to the reaction mixture (AA supernatant; red line) and the other without addition of β-chitin (*Pp*AA10 supernatant grey line). The IR spectrum of β-chitin can be analyzed considering two different regions of the spectrum, namely the "sugar fingerprint" region (1,500–950 cm^{-1}), which is fundamental for the identification and the structural characterization of polysaccharides, and the region of the functional groups (2,500–3,600 cm^{-1}), which gives information on the crystallinity of the sample. The fingerprint region contains bands assigned to sugar ring C—C and C—O vibration modes (1,109 and 1,064 cm^{-1}, respectively), as well as the antisymmetric stretching of C1—O—C4 moiety of the glycosidic linkage in chitin (1,154 cm^{-1}).[39–41] Other characteristic peaks include the C=O stretching (amide I 1,637 cm^{-1}) and the C—N stretching modes, together with the N—H bending (amide II 1,545 cm^{-1}) of the chitin acetylamide group.[42] A further band of CH$_2$ scissoring at 1,430 cm^{-1} is known as a marker of crystallinity.[40] Finally, the bands between 3,400 and 3,270 cm^{-1} are attributed to O—H and N—H stretching, respectively of the C=O----H—N or C=O----H—O moieties for the intra-sheet hydrogen bond in crystalline chitin.[42,43] The spectrum of the digestion supernatants shows the same fingerprint features (the bands at 1,154, 1,109, and 1,064 cm^{-1}),

which are consistent with the presence of oligosaccharides produced by the lytic action of *Pp*AA10 on β-chitin (Figure 4a, blue line), in agreement with the MALDI-TOF results presented above (Figure 3). Indeed, the shape of the fingerprints peaks of β-chitin and its oligosaccharides are expected to be conserved upon digestion, despite some changes in the 3,200–3,400 cm^{-1} region due to alteration of the hydrogen bonding network with respect to crystalline β-chitin.[41] The absence of the water solvent allows a clear visualization of the sugar spectral bands, however the intense band at 3300 cm^{-1} can be attributed to the small amount of water retained within the samples after the drying step, which also hampers a detailed analysis of the region 3,200–3,400 cm^{-1} of the spectrum. These oligosaccharides are composed of *N*-acetyl-glucosamines (NAGs) units with different degree of polymerization, which are among the most abundant soluble degradation products of β-chitin digested by PMOs.[3] The bands at 1,637 cm^{-1} and 1,545 cm^{-1} can therefore be assigned to the acetyl groups of NAGs, in particular to C=O and N—H vibrations, respectively. The presence of the latter band indicates that no deacetylation of NAG occurred during digestion.[42] Furthermore, the band at 1,730 cm^{-1} can be assigned to the C=O stretching of the hydrogen-bonded carboxylic acid groups (—COOH) of aldonic acid
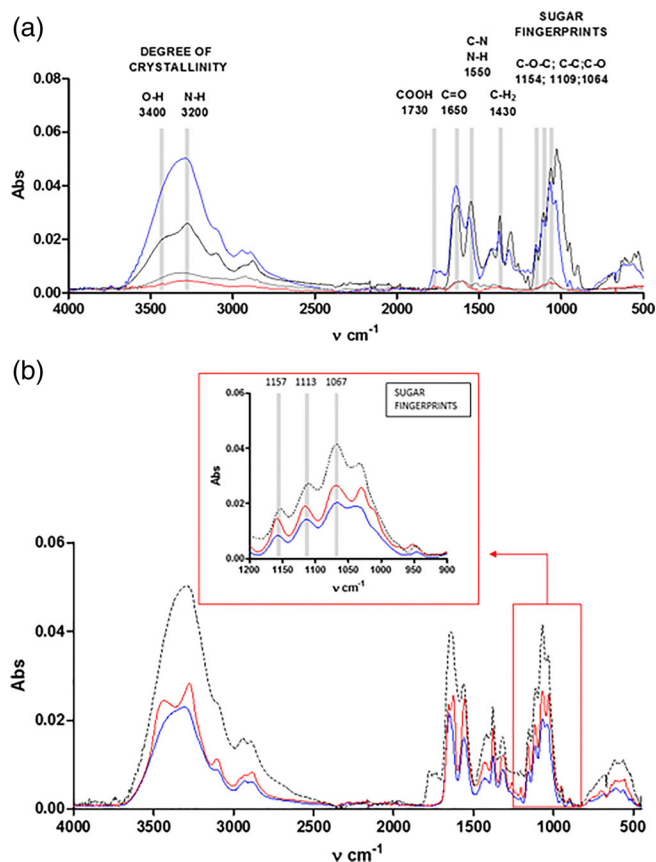
FIGURE 4 (a) ATR-FTIR spectrum of β-chitin powder (black line), AA supernatant (red line), *Pp*AA10 supernatant (grey line) and the digestion supernatant (blue line). IR bands are labeled in the picture; of particular interest is the glycosidic bond vibration band at 1,154 cm^{-1}. (b) ATR-FTIR spectrum of 1 mM NAG$_3$ (blue line), 1 mM NAG$_6$ (red line), and digested supernatant (black dotted line) in water plus 1 mM ascorbic acid. The IR bands due to the glycosidic bond are highlighted in the inset

moieties, generated in the oligosaccharides by the oxidative action of the enzyme (Figure 4a, blue line).[35,44] This feature is characteristic of the oxidized oligosaccharide and therefore a marker of the PMO activity. Conversely, in case of C4-specific PMOs activity we would not expect the band at 1,730 cm^{-1} due to the conversion of the ketoaldose into a gemdiol aldose lacking of any carbonylic or carboxylic groups. Finally, the spectra obtained for the control samples AA and *Pp*AA10 supernatants (Figure 4a, red and grey traces, respectively) only display low intensity and broad bands, which do not show the sugar features of the digested samples. Altogether, these observations indicate that chitin degradation by PMOs can readily be monitored by ATR-FTIR spectroscopy.

In order to corroborate the bands assignment in the digested sample, ATR-FTIR measurements were also performed on control solutions containing NAG$_3$ and NAG$_6$

chito-oligosaccharides (Figure 4b). The spectra of both oligosaccharides feature the same pattern in the sugar fingerprints region, with the bands at 1,157, 1,113, and 1,064 cm^{-1} that are superimposable with those found in the spectra of the digested supernatants. On the other hand, here the carboxylic acid C=O stretching (1,730 cm^{-1}) is not present, as these native oligosaccharides are not oxidized at position C1 of the ring. Moreover, the spectra of the native oligosaccharides differ from that of the solid β-chitin particularly in the 3,200–3,400 cm^{-1} region. In fact, chitin crystal structures reveal that the chitin chains are organized in sheets where they are tightly held by a number of intra-sheet hydrogen bonds.[45] Therefore, in solid chitin the vibration bands at 3,200 cm^{-1} and 3,400 cm^{-1} for N—H and C=O stretching, respectively, are attributed to full intermolecular C—O----H—N or C=O----H—O intra-sheet hydrogen bonding.[42,43] Conversely, the action of *Pp*AA10 produces a blend solution of oligosaccharides (digested samples) (DP4–DP8 from MALDI-TOF analysis, Figure 3) that gives rise to a different pattern of bands at 3200 and 3,440 cm^{-1} similar to the ones for NAG$_{3/6}$, most probably due to the vibrations of the free O—H and N—H groups. Because of this variability, in order to discriminate which substrate a specific PMO enzyme is active on, it is more appropriate to observe the fingerprint region of the spectrum, which unambiguously allows the identification of the different oligosaccharides.

As a demonstration of the applicability of this method, the activity of *Pp*AA10 was also tested on cellulose and starch as polysaccharide substrates. The spectra of the digested supernatants (Figure 5a) show that the enzyme is active only on β-chitin, since the corresponding spectrum is the only one that contains the sugar fingerprint bands. The same method was also applied to the *Aspergillus Oryzae* PMO from the AA11 family (*Ao*AA11), characterized elsewhere and with known chitinolytic activity.[46] The spectrum obtained after an overnight reaction at 50°C, shown in Figure 5b, reveals sugar fingerprints typical of soluble oligosaccharides only in the presence of β-chitin.

Next, a scale up of the reaction on a complex polysaccharide matrix was performed. Squid pen was washed and ground, then used as a substrate without being subjected to any aggressive treatment or purification step. A reaction batch in the presence of *Pp*AA10 was set up together with a control reaction in which commercial β-chitin was used, while the duration of the digestion was extended to 48 h. As shown in Figure 5c, the two spectra share the same IR spectral features, which are indeed comparable with those of the experiments described above, further confirming the robustness of the proposed ATR-IR based approach.
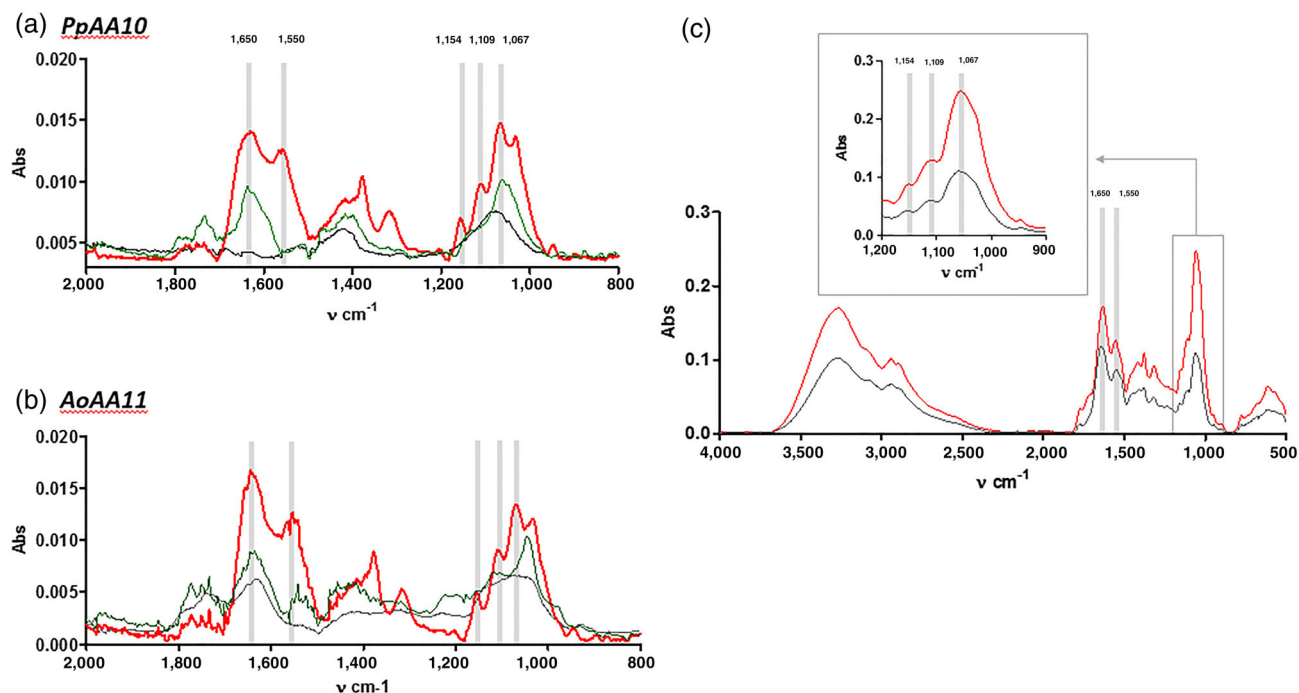
FIGURE 5 (a) ATR-FTIR spectra of the supernatants obtained after overnight digestion at 50°C of β-chitin (red), cellulose (green), and starch (black) by *Pp*AA10 in water in presence of 1 mM ascorbic acid. (b) ATR-FTIR spectra of the supernatants obtained after overnight digestion at 50°C of β-chitin (red), cellulose (green), and starch (black) by *Ao*AA11 PMO in water in presence of 1 mM ascorbic acid. (c) ATR-FTIR spectra of the supernatants obtained after 48 h digestion at 50°C of β-chitin (red), and squid pen from a complex matrix (grey) by *Pp*AA10 in water in presence of 1 mM ascorbic acid and of chitinase from *Streptomyces griseus*

Finally, a comprehensive set of control samples was prepared as well, in order to confirm the significance of the obtained results. Spectra of the supernatants obtained after overnight digestion at 50°C without the addition of substrate and without the addition of *Pp*AA10 are summarized in Figure S8. Here it can be seen that when the protein is not active on a specific substrate, the fingerprints region is lacking the "three bands pattern" (1,157, 1,113, and 1,064 cm^{-1}), matching the features of the supernatant spectrum obtained without the addition of substrate, which is also similar to the spectrum of the sole protein *Pp*AA10 that did not undergo incubation at 50°C (Figure S9). Similarly, to the experiment with *Pp*AA10, control samples were also prepared for reactions carried out with *Ao*AA11 and the resulting spectra are depicted in Figure S10.

3 | CONCLUSIONS

In this work, we characterized a novel chitin-active PMO enzyme belonging to the AA10 family from the bacterium *P. putida*. This enzyme was exploited as a model system to develop a simple but sensitive assay for PMOs activity and substrate specificity based on the detection of soluble oligosaccharides as reaction products with ATR-FTIR spectroscopy. Although being limited to the

detection of the soluble fraction of the products, this methodology profitably supports the standard PMO activity assays. Indeed, because of its simplicity and cost-effectiveness, it can be used as a first screening test to determine possible substrates for the PMO under investigation before moving to more accurate, though time-consuming, chromatographic or mass spectrometry methods.

4 | MATERIALS AND METHODS

4.1 | Chemicals, materials, and microorganism strains

Oligonucleotide primers and synthetic genes were purchased from Eurofins (Germany) and IDT (Integrated DNA Technologies, Inc.), respectively. All PCR reactions were performed using a Phusion™ High-Fidelity DNA Polymerase (ThermoFisher). Chemicals were purchased from Merck (Germany), Sigma-Aldrich (USA), or Thermo Scientific (USA), if not stated otherwise. *Escherichia coli* DH5α and BL21(DE3) strains (New England Biolabs) were used for the cloning step and to produce the recombinant *Pp*AA10, respectively. β-chitin from squid pen was purchased from Chitin France, NAG$_3$ (Triacetylchitotriose), and NAG$_6$ (Hexacetylchitohexaose) were purchased from Megazyme.

4.2 | *P. putida* AA10 sequence analysis

The target protein (*Pp*AA10) was identified in the CAZy database[1] among the nearly 5,877 uncharacterized bacterial AA10 PMO sequences. The protein sequence (UniProt ID: B1J2U9) is 211 amino acids in length. While the function of the first 18 residues of the sequence remains unknown, the amino acids 19–206 were classified by InterPro automatic annotation as a chitin-binding domain belonging to the PMO_10 Pfamily (PF03067). Moreover, a multiple alignment of the residues 19–211 with other characterized AA10s revealed that the histidine in position 19 corresponds to the catalytic histidine 1 of the mature protein. The alignment (Figure S6) has been calculated with the Clustal Omega bioinformatic tool.

4.3 | Gene construction and protein production in *E. coli*

The nucleotide sequence of *Pp*AA10 was taken from the annotated genome of *P. putida—strain W619* available in the GenBank database (NC_010501.1). In order to obtain an active *Pp*AA10, the constitutive signal peptide was excluded for avoiding incorrect post-translational processing and an N-terminal cleavable His-tag sequence was added for improving the yield and facilitating the purification of the protein.[28,29] Considering the importance of the His1, α-aminogroup and side-chain for the copper-binding and catalysis, its cleavability was strategic. Thus the gene construct coding for the mature form of the protein, suitable for Ligation Independent Cloning (LIC) with the aLICator® system (ThermoFisher), was designed by adding specific 5′ and 3′ sequences overhanging the pLATE52 vector which includes a 6xHis coding sequence at the N-terminal. The following primers for PCR amplification were used: Primer forward: 5′—GGTT GGGAATTGCAACATGGTTCGATTGCGAGCCCA—3′; Primer Reverse: 5′ - GGAGATGGGAAGTCATTAC TTGGCAACGAAATTGAGATCG—3′. The LIC method was applied to generate a *PpAA10*-pLATE52 plasmid, which was then used to transform an aliquot of competent DH5α *E. coli* cells. Positive colonies were identified by colony-PCR and grown overnight at 37°C in a shaking incubator at 250 rpm. A minipreparation of plasmid DNA was carried out to extract and purify the *PpAA10*-pLATE52 vector. The resulting construct (Figure S11) was used to transform BL21(DE3) *E. coli* cells. The *Pp*AA10 protein was produced in BL21(DE3) *E. coli* cells in a 4×1 L of LB culture, shaking at 250 rpm and 37°C. Once the sample reached an OD_{600} of 0.8, protein expression was induced by adding isopropyl β-D-1-thiogalactopyranoside (IPTG) to

a final concentration of 0.5 mM, and lowering the shaking speed to 200 rpm and the temperature to 25°C. The cells were harvested after 18 h by centrifugation at 4500*g* for 20 min at 4°C. The cell paste was then resuspended in three volumes of 50 mM Tris–HCl pH 8.0, 200 mM NaCl, 30 mM Imidazole (Buffer A) and eventually sonicated on ice with a Microson Ultrasonic cell disruptor for 45 min. The His-tagged protein was loaded on a 5-ml HisTrap FF Crude (Amersham Bioscience) column equilibrated in Buffer A, then collected by gradient elution with 50 mM Tris–HCl pH 8.0, 200 mM NaCl, 300 mM Imidazole (Buffer B). Peak fractions were concentrated to 2 mL by means of an Amicon Ultrafiltration apparatus with a 10 kDa molecular weight cutoff membrane filter. The concentrated protein was loaded on a Superdex 75 column equilibrated with 50 mM Tris–HCl pH 7.5, 150 mM NaCl for size-exclusion chromatography. Protein concentration was determined by measuring the $A_{280\ nm}$ with an extinction coefficient of 47,440 M^{-1} cm^{-1} and a molecular weight of 25,014.84 Da for His-tagged *Pp*AA10 (theoretical parameters were calculated with the ExPASy ProtParam tool).

4.4 | Cleavage with WELQut® protease and copper loading

In order to remove the histidine tag and the pLATE52-specific N-terminal sequence, different conditions for protein cleavage with a WELQut® Protease were tested. Finally, large-scale cleavage of *Pp*AA10 was carried out with a 1:50 WELQut®/*Pp*AA10 ratio at 23°C for 3 h. The sample was then passed on a 5-ml HisTrap FF Crude (Amersham Bioscience) column to remove the WELQut® protease and the residual uncleaved *Pp*AA10. The efficiency of the reaction was assessed by SDS-PAGE, while protein concentration was determined by measuring the $A_{280\ nm}$ with an extinction coefficient of 41,900 M^{-1} cm^{-1} and a molecular weight of 21,908.4 Da (theoretical parameters were calculated with the ExPASy ProtParam tool). Finally, the protein was copper loaded by adding three equivalents of $CuSO_4 \cdot 5H_2O$ for 1 h at room temperature. The mixture was then applied to a G25 Sephadex column material to remove the Cu in excess. The eluted protein was used for further analysis.

4.5 | EPR spectroscopy

Continuous wave (CW) X-band EPR spectra of *Pp*AA10 samples in frozen solution were acquired on a Bruker micro EMX spectrometer operating at ~9.30 GHz and 170 K, with a modulation amplitude of 4 G and microwave

power of 10.02 mW. EPR spectra were collected at different pH values and protein concentrations, before and after addition of substrate. The *Pp*AA10 concentration was 0.21 mM in 50 mM TRIS buffer, 200 mM NaCl, pH 7.0. For the titration experiments, the buffer was exchanged to a "multibuffer" solution containing sodium acetate, MES, HEPES, TRIS, and CHES (10 mM each), 200 mM NaCl and the pH adjusted with small additions of 1 M HCl or 1 M NaOH solutions. The pH was monitored directly into the protein sample solution using an InLab® micro pH electrode from Mettler Toledo connected to a Radiometer Analytical ION450® pH-meter calibrated by standard buffer solutions at pH values of 4.01, 7.00, and 10.01. Spectral simulations were performed using the software Easyspin 5.2.18 integrated into MatLab 2017a.[47]

4.6 | Activity assays

*Pp*AA10 was incubated with β-chitin. Protein activity was assessed by analyzing oxidized products with MALDI-TOF mass spectrometry. One hundred microliter digestion reactions were set up with 0.2% w/v substrate, 1 μM *Pp*AA10, 10 mM ammonium acetate pH 6.0 and 1 mM AA. Reaction tubes were incubated overnight at 30°C, shaking at 250 rpm. The solid substrate was then removed by centrifugation for 5 min at 14,000 rpm at 4°C and the supernatant was collected for subsequent analysis. Samples for MALDI-TOF analysis were prepared by mixing 1 μl of the supernatant liquid with an equal volume of a solution of 10 mg/ml 2,5-dihydroxybenzoic acid in 50% v/v acetonitrile, 0.1% v/v trifluoroacetic acid directly on a SCOUT-MTP 384 target plate (Bruker). The spotted samples were then allowed to dry on the bench for 10–15 min before performing the mass spectrometry measurements on an Ultraflex III MALDI-TOF instrument (Bruker).

4.7 | ATR-FTIR spectroscopy

Reaction samples were prepared by suspending 1 mg of β-chitin in 100 μl of an unbuffered aqueous (Milli-Q®) solution containing 1 mM AA and 1 μM *Pp*AA10. Reaction tubes were incubated at 50°C and 250 rpm overnight. The digested suspension was then centrifuged at 14,000 rpm for 5 min to separate the unreacted solid β-chitin. An aliquot of 4 μl of the supernatant, which contains the oligosaccharides produced by digestion of β-chitin by *Pp*AA10 (digested supernatant hereafter), was loaded on the crystal and air dried for 5 min to eliminate water. In addition, two control samples were prepared following the same procedure as above: one

was obtained without addition of *Pp*AA10 to the reaction mixture, thus containing only AA, as chitin is insoluble in water; and the other one without addition of β-chitin, containing *Pp*AA10 and AA, but not the processed substrate. ATR-FTIR spectra were collected using a Perkin Elmer Spectrum TWO UTR-FTIR with PerkinElmer® Spectrum IR software, version 10.6.0.893. To improve the signal-to-noise ratio for each spectrum, 32 interferograms with a spectral resolution of ± 4 cm^{-1} were averaged. Background spectra, which were collected under identical conditions, were subtracted from the sample spectra.[48–50]

AUTHOR CONTRIBUTIONS

Ilenia Serra: Data curation (supporting); formal analysis (supporting); investigation (supporting); methodology (supporting); writing – original draft (supporting); writing – review and editing (supporting). **Daniele Piccinini:** Data curation (supporting); formal analysis (supporting); methodology (supporting). **Giulia Di Rocco:** Conceptualization (lead); data curation (lead); methodology (lead); writing – original draft (lead). **Alessandro Paradisi:** Data curation (lead); supervision (supporting); writing – review and editing (supporting). **Luisa Ciano:** Conceptualization (equal); data curation (equal); supervision (equal); writing – review and editing (equal). **Marzia Bellei:** Data curation (equal); formal analysis (equal). **Carlo Augusto Bortolotti:** Supervision (equal); writing – review and editing (equal). **Gianantonio Battistuzzi:** Visualization (equal); writing – review and editing (equal). **Marco Sola:** Visualization (equal); writing – review and editing (equal). **Paul Howard Walton:** Supervision (equal); writing – original draft (equal); writing – review and editing (equal).

ORCID

Giulia Di Rocco https://orcid.org/0000-0002-3187-2210

REFERENCES

1. Lombard V, Golaconda Ramulu H, Drula E, Coutinho PM, Henrissat B. The carbohydrate-active enzymes database (CAZy) in 2013. Nucleic Acids Res. 2014;42:490–495.

2. Levasseur A, Drula E, Lombard V, Coutinho PM, Henrissat B. Expansion of the enzymatic repertoire of the CAZy database to integrate auxiliary redox enzymes. Biotechnol Biofuels. 2013;6: 1–14.

3. Vaaje-kolstad G. An oxidative enzyme boosting the enzymatic conversion of recalcitrant polysaccharide. Science. 2010;330: 219–223.

4. Forsberg Z, Sørlie M, Petrović D, et al. Polysaccharide degradation by lytic polysaccharide monooxygenases. Curr Opin Struct Biol. 2019;59:54–64.

5. Simmons TJ, Frandsen KEH, Ciano L, et al. Structural and electronic determinants of lytic polysaccharide monooxygenase reactivity on polysaccharide substrates. Nat Commun. 2017;8: 1064.

6. Couturier M, Ladevèze S, Sulzenbacher G, et al. Lytic xylan oxidases from wood-decay fungi unlock biomass degradation. Nat Chem Biol. 2018;14:306–310.

7. Vu VV, Beeson WT, Span EA, Farquhar ER, Marletta MA. A family of starch-active polysaccharide monooxygenases. Proc Natl Acad Sci. 2014;111:13822–13827.

8. Sabbadin F, Urresti S, Henrissat B, et al. Secreted pectin monooxygenases drive plant infection by pathogenic oomycetes. Science (80-). 2021;373:774–779.

9. Walton PH, Davies GJ. On the catalytic mechanisms of lytic polysaccharide monooxygenases. Curr Opin Chem Biol. 2016; 31:195–207. https://doi.org/10.1016/j.cbpa.2016.04.001.

10. Borisova AS, Isaksen T, Dimarogona M, et al. Structural and functional characterization of a lytic polysaccharide monooxygenase with broad substrate specificity. J Biol Chem. 2015; 290:22955–22969.

11. Bertini L, Breglia R, Lambrughi M, et al. Catalytic mechanism of fungal lytic polysaccharide monooxygenases investigated by first-principles calculations. Inorg Chem. 2018;57:86–97.

12. Chylenski P, Bissaro B, Sørlie M, et al. Lytic polysaccharide monooxygenases in enzymatic processing of lignocellulosic biomass. ACS Catal. 2019;9:4970–4991.

13. Johansen KS. Discovery and industrial applications of lytic polysaccharide mono-oxygenases. Biochem Soc Trans. 2016;44: 143–149.

14. Quinlan RJ, Sweeney MD, Lo Leggio L, et al. Insights into the oxidative degradation of cellulose by a copper metalloenzyme that exploits biomass components. Proc Natl Acad Sci U S A. 2011;108:15079–15084.

15. Ciano L, Davies GJ, Tolman WB, Walton PH. Bracing copper for the catalytic oxidation of C–H bonds. Nat Catal. 2018;1: 571–577.

16. Vaaje-Kolstad G, Forsberg Z, Loose JS, Bissaro B, Eijsink VG. Structural diversity of lytic polysaccharide monooxygenases. Curr Opin Struct Biol. 2017;44:67–76.

17. Kuusk S, Bissaro B, Kuusk P, et al. Kinetics of H2O2-driven degradation of chitin by a bacterial lytic polysaccharide monooxygenase. J Biol Chem. 2018;293:523–531.

18. Hangasky JA, Iavarone AT, Marletta MA. Reactivity of O2 versus H2O2 with polysaccharide monooxygenases. Proc Natl Acad Sci U S A. 2018;115:4915–4920.

19. Kittl R, Kracher D, Burgstaller D, Haltrich D, Ludwig R. Production of four neurospora crassa lytic polysaccharide monooxygenases in Pichia pastoris monitored by a fluorimetric assay. Biotechnol Biofuels. 2012;5:79.

20. Filandr F, Man P, Halada P, Chang H, Ludwig R, Kracher D. The H2O2-dependent activity of a fungal lytic polysaccharide monooxygenase investigated with a turbidimetric assay. Biotechnol Biofuels. 2020;13:37. https://doi.org/10.1186/s13068-020-01673-4.

21. Wang D, Li J, Wong ACY, Aachmann FL, Hsieh YSY. A colorimetric assay to rapidly determine the activities of lytic polysaccharide monooxygenases. Biotechnol. Biofuels. 2018;11:215. https://doi.org/10.1186/s13068-018-1211-z.

22. Breslmayr E, Hanžek M, Hanrahan A, et al. A fast and sensitive activity assay for lytic polysaccharide monooxygenase. Biotechnol. Biofuels. 2018;11:1–13. https://doi.org/10.1186/s13068-018-1063-6.

23. Breslmayr E, Daly S, Požgajčić A, et al. Improved spectrophotometric assay for lytic polysaccharide monooxygenase. Biotechnol Biofuels. 2019;12:1–12. https://doi.org/10.1186/s13068-019-1624-3.

24. Westereng B, Arntzen M, Agger JW, Vaaje-Kolstad G, Eijsink VGH. Analyzing activities of LPMO by liquid chromatography and mass spectrometry. Methods Mol Biol. 2017;1588: 209–214. https://doi.org/10.1007/978-1-4939-6899-2_7.

25. Bissaro B, Røhr ÅK, Müller G, et al. Oxidative cleavage of polysaccharides by monocopper enzymes depends on H(2)O(2). Nat Chem Biol. 2017;13:1123–1128.

26. Hangasky JA, Iavarone AT, Marletta MA. Reactivity of O2 versus H2O2 with polysaccharide monooxygenases. Proc Natl Acad Sci. 2018;115(19):4915–4920.

27. Paradisi A, Johnston EM, Tovborg M, et al. Formation of a copper(II)-tyrosyl complex at the active site of lytic polysaccharide monooxygenases following oxidation by H2O2. J Am Chem Soc. 2019;141:18585–18599.

28. Wijekoon CJK, Ukuwela AA, Wedd AG, Xiao Z. Evaluation of employing poly-lysine tags versus poly-histidine tags for purification and characterization of recombinant copper-binding proteins. J Inorg Biochem. 2016;162:286–294. https://doi.org/10.1016/j.jinorgbio.2015.12.009.

29. Kadowaki MAS, Magri S, de Godoy MO, Monclaro AV, Zarattini M, Cannella D. A fast and easy strategy for lytic polysaccharide monooxygenase-cleavable His6-Tag cloning, expression, and purification. Enzyme Microb Technol. 2021;143: 109704. https://doi.org/10.1016/j.enzmictec.2020.109704.

30. Hemsworth GR, Taylor EJ, Kim RQ, et al. The copper active site of CBM33 polysaccharide oxygenases. J Am Chem Soc. 2013;135:6069–6077.

31. Forsberg Z, Røhr ÅK, Mekasha S, et al. Comparative study of two chitin-active and two cellulose-active AA10-type lytic polysaccharide monooxygenases. Biochemistry. 2014;53:1647–1656.

32. Courtade G, Ciano L, Paradisi A, et al. Mechanistic basis of substrate-O2 coupling within a chitin-active lytic polysaccharide monooxygenase: An integrated NMR/EPR study. Proc Natl Acad Sci U S A. 2020;117:19178–19189.

33. Iwaizumi M, Kudo T, Kita S, et al. Correlation between the hyperfine coupling constants of donor nitrogens and the structures of the first coordination sphere in copper complexes as studied by 14N ENDOR spectroscopy. Inorg Chem. 1986;25: 1546–1550.

34. Frandsen KEH, Simmons TJ, Dupree P, et al. The molecular basis of polysaccharide cleavage by lytic polysaccharide monooxygenases. Nat Chem Biol. 2016;12:298–303.

35. Bissaro B, Isaksen I, Vaaje-Kolstad G, Eijsink VGH, Røhr ÅK. How a lytic polysaccharide monooxygenase binds crystalline chitin. Biochemistry. 2018;57(12):1893–1906. https://doi.org/10.1021/acs.biochem.8b00138.

36. Peisach J, Blumberg WE. Structural implications derived from the analysis of electron paramagnetic resonance spectra of natural and artificial copper proteins. Arch Biochem Biophys. 1974;165:691–708. https://www.sciencedirect.com/science/article/pii/0003986174902987.

37. Chaplin AK, Wilson MT, Hough MA, et al. Heterogeneity in the histidine-brace copper coordination sphere in auxiliary activity family 10 (AA10) lytic polysaccharide monooxygenases. J Biol Chem. 2016;291:12838–12850.

38. Hemsworth GR, Johnston EM, Davies GJ, Walton PH. Lytic polysaccharide monooxygenases in biomass conversion. Trends Biotechnol. 2015;33:747–761. https://doi.org/10.1016/j.tibtech.2015.09.006.

39. Sekkal M, Dincq V, Legrand P, Huvenne JP. Investigation of the glycosidic linkages in several oligosaccharides using FT-IR and FT Raman spectroscopies. J Mol Struct. 1995;349:349–352.

40. Synytsya A, Novak M. Structural analysis of glucans. Ann Transl Med. 2014;2:1–14.

41. Prabu K, Natarajan E. Isolation and FTIR spectroscopy characterization of chitin from local sources. Adv Appl Sci Res. 2012;3:1870–1875. www.pelagiaresearchlibrary.com.

42. Rinaudo M. Chitin and chitosan: Properties and applications. Prog Polym Sci. 2006;31:603–632.

43. Marchessault RH, Pearson FG, Liang CY. Infrared spectra of crystalline polysaccharides. Biochim Biophys Acta. 1960;45:499–507.

44. Naumann D, Barnickel G, Bradaczek H, Labischinski H, Giesbrecht P. Infrared spectroscopy, a tool for probing bacterial peptidoglycan. Eur J Biochem. 1982;125:505–515.

45. Sikorski P, Hori R, Wada M. Revisit of α-chitin crystal structure using high resolution X-ray diffraction data. Biomacromolecules. 2009;10:1100–1105.

46. Hemsworth GR, Henrissat B, Davies GJ, Walton PH. Discovery and characterization of a new family of lytic polysaccharide mono-oxygenases. Nat Chem Biol. 2014;10:122–126. https://doi.org/10.1038/nchembio.1417.

47. Stoll S, Schweiger A. EasySpin, a comprehensive software package for spectral simulation and analysis in EPR. J Magn Reson. 2006;178:42–55.

48. Forsberg Z, Nelson CE, Dalhus B, et al. Structural and functional analysis of a lytic polysaccharide monooxygenase important for efficient utilization of chitin in Cellvibrio japonicus. J Biol Chem. 2016;291:7300–7312.

49. Forsberg Z, Mackenzie AK, Sørlie M, et al. Structural and functional characterization of a conserved pair of bacterial cellulose-oxidizing lytic polysaccharide monooxygenases. Proc Natl Acad Sci U S A. 2014;111:8446–8451.

50. Kruer-Zerhusen N, Alahuhta M, Lunin VV, Himmel ME, Bomble YJ, Wilson DB. Structure of a Thermobifida fusca lytic polysaccharide monooxygenase and mutagenesis of key residues. Biotechnol Biofuels. 2017;10:1–12.

SUPPORTING INFORMATION

Additional supporting information may be found in the online version of the article at the publisher's website.